# Supporting Information

## Huang et al. 10.1073/pnas.1207946109

### SI Results

Fig. S8 shows group-average maps for eight subjects who participated in additional two-condition experiments designed to map shoulder, arm, leg, and toe representations in the primary somatosensory cortex. Contrasting random air-puff stimulation on both shoulders with no stimulation only activated a region within the parietal shoulder area mapped in the original "lips vs. shoulders" experiments (Fig. S8*A*). The extent of the shoulder representations in both the new and original experiments did not extend further into the postcentral gyrus. Similarly, contrasting random air-puff stimulations on both arms with no stimulation only activated a portion of the original parietal shoulder area, and no significant activation was found in the postcentral gyrus (Fig. S8*B*). Our second attempt at using air-puff stimuli with the "stimulation on vs. off" paradigm failed to find representations of shoulders and arms in the postcentral gyrus. Further studies are required to find more effective tactile stimuli for automatic stimulation on the shoulders and arms.

Brushing stimulation on the side of the left leg activated a wider region encompassing part of the primary somatosensory cortex (S-I) in the postcentral gyrus and superior parietal lobule in the right hemisphere (Fig. S8*C*). The posterior part of this region overlaps with the parietal leg area activated by air-puff stimulations in the original "face vs. legs" experiments. Brushing stimulation on all toes resulted in much stronger activation in a wider region encompassing the primary motor cortex (M-I) in the precentral gyrus, the primary somatosensory cortex (S-I) in the postcentral gyrus, and the superior parietal lobule in both hemispheres (Fig. S8*D*). The posterior part of this region also overlaps with the parietal toe area activated by air-puff stimulations in the original "fingers vs. toes" experiments. The activations in the primary motor cortex likely resulted from small, passive movements of the toes generated by the brush during stimulation periods. The S-I representation of toes activated by brushing stimulation suggests that the unusual area in the central sulcus originally activated by air-puff stimulation on the toes (Figs. S2*D*, S4*D*, and S5) could be the M-I representation of fingers. It is likely that passive tactile stimulation on the fingers resulted in suppression of neural activity in the unstimulated M-I representation of fingers in the central sulcus, with rebound of neural activity during passive stimulation on the toes; this resulted in apparent activation in the central sulcus that was positively correlated with activation in the parietal toe area. Further experiments are required to study the effect that specific pairings of body parts has on activation maps.

One limitation of the present study is that our methods cannot functionally separate a body-part representation if the activation extends continuously from the primary somatosensory cortex (S-I) into the posterior parietal cortex (Brodmann's areas 5 and 7). We have proposed a schematic model to assist with the interpretation of activation extents driven by different modalities of stimuli in terms of Brodmann areas (Fig. S9). As shown in this model, the parietal leg/toe areas activated by air-puff stimulation overlap with the posterior parts of regions (Brodmann's area 2) driven by brushing stimulation and with the anterior parts of regions (Brodmann's area 5) driven by looming stimuli. This finding suggests that the parietal leg and toe areas are not simply primary somatosensory cortex, but also include part of the posterior parietal cortex.

### SI Methods

**Supplementary Experiments.** Eight subjects participated in four additional two-condition paradigms designed to map the representations of shoulders, arms, legs, and toes in the primary somatosensory cortex. Each paradigm was scanned twice in the same functional session. In each 256-s scan, tactile stimuli were delivered to one body part for 16 s followed by 16 s of no stimulation repeatedly. As it is difficult to apply manual stimulation to the subject's shoulders and arms located deep inside the MRI scanner, computer-controlled air puffs (200-ms pulses) were randomly delivered to 12 sites on both shoulders (or both arms) via the tactile stimulation suit for 16 s followed by 16 s of no stimulation (Fig. S8 *A* and *B*). In the other two paradigms, an experimenter followed the timing of computer-controlled fiber optic lights and used an MR-compatible paint brush (2-in wide) to apply gentle brushing stimulation to the side of the left leg (or to all toes) for 16 s followed by 16 s of no stimulation (Fig. S8 *C* and *D*).

**Image Acquisition and Parameters.** Subjects were scanned with eight-channel head coils in General Electric 3-Tesla MRI scanners in the functional MRI (fMRI) Center of University of California at San Diego. Functional images were collected during 256-s or 512-s scans with the following parameters: single-shot echo-planar images (EPI), field of view (FOV) = 20 cm, 3.125 × 3.125-mm in-plane, 3.5-mm thick slices, 31 axial slices, 64 × 64 matrix, flip angle = 90°, TE = 30 ms, TR = 2,000 ms, and 128 or 256 images per slice. Functional images of the supplementary experiments were acquired with slightly different parameters: single-shot EPI, FOV = 22.4 cm, 3.5 × 3.5 mm in-plane, 3.5-mm thick slices, 38 axial slices, 64 × 64 matrix, flip angle = 90°, TE = 30.1 ms, TR = 2000 ms, and 128 images per slice.

Two sets of structural images (FSPGR, FOV = 25.6 cm, 1 × 1 mm in-plane, 1-mm thick slices, 160–170 axial slices, 256 × 256 matrix) for cortical surface reconstruction (see below) and registration between functional and structural images were collected at the same plane as functional images in the first session of each subject. Alignment images for registration between functional and structural images (FSPGR, FOV = 25.6 cm, 1 × 1 mm in-plane, 1.3-mm thick slices, 106 axial slices, 256 × 256 matrix) were collected at the same plane as functional images in succeeding sessions of the same subject.

**Structural Image Analysis.** The FreeSurfer package (1, 2) was used to reconstruct cortical surfaces from the average of two sets of structural images for each subject. The structural images (1 × 1 × 1 mm) in the first session or alignment images (1 × 1 × 1.3 mm) in the succeeding sessions of the same subject were then used to register functional images with his/her cortical surfaces using FreeSurfer. The Montreal Neurological Institute Automated Linear Registration Package (3) was used to generate Talairach transformation matrices for structural images.

**Functional Image Analysis.** For each session, functional images were motion-corrected and registered to the last functional scan using the 3dvolreg function of the AFNI package (http://afni.nimh.nih.gov/afni) and then registered with the cortical surfaces using the alignment images in FreeSurfer. In each tactile mapping session (including supplementary experiments), point-wise time average was applied to two motion-corrected scans of the same paradigm. In each visual mapping session, the time courses of the two clockwise scans were reversed before they were averaged

with the time courses of the other two counterclockwise scans (see *Visual Mapping Paradigm* in the main text).

A fast Fourier transform was performed on the average time courses (128 or 256 time points) of each voxel after removing the linear trend. A complex number (real and imaginary) was obtained at each frequency bin on the Fourier spectrum. An *F*-statistic value was obtained by comparing power at the stimulus frequency (eight cycles per scan) to the sum of power at the remaining frequencies (excluding 1–3, 7, 9, 15–17, 23–25, and 32 cycles per scan) in the Fourier spectrum. For each voxel, an uncorrected *P* value was estimated by considering the degrees of freedom (*df*) of signal ($df = 2$) and noise ($df = 102$ for 128 time points; $df = 230$ for 256 time points). The phase angle, θ, of each voxel was also computed by combining the real and imaginary components at the stimulus frequency (eight cycles per scan) on the Fourier spectrum. For each voxel, a complex number ($F_r$, $F_i$) incorporating both *F*-statistic and phase values was computed by $F_r = f\cos(\theta)$ and $F_i = f\sin(\theta)$, where *f* is the square root of the *F*-statistic value. In two-condition block-design scans, regions with phase angles falling into the first and second halves of a cycle were rendered in two different colors on the cortical surfaces (Fig. 2 and Fig. S2). For example, regions activated during face stimulation were rendered in red, and regions activated during finger stimulation were rendered in green. In phase-encoded visual mapping scans, the phase angle was rendered using a continuous half color wheel (red → blue → green for upper → horizontal → lower fields) for the left or right visual hemifield (Fig. 3 and Figs. S5 and S7).

**Spherical Group Average.** Single-subject maps bearing *F*-statistic and phase values ($F_r$, $F_i$) were averaged across all available subjects for each paradigm using spherical group-average methods (4). The inflated cortical surfaces of the left and right hemispheres were further inflated into spherical coordinates and then morphed to register with the average sphere for the left and right hemisphere, respectively. The complex number ($F_r$, $F_i$) of each vertex from each subject's morphed spherical surface was sampled on the average sphere, and the numbers were averaged across subjects on the common spherical coordinates. The resulting complex numbers of statistics on the average spheres were reverse-sampled back to subject 1's morphed spheres, which allowed group-average statistics to be displayed as single-subject statistics on inflated cortical surfaces of a representative subject (Fig. 3 and Figs. S4 and S5).

**Surface-Based Regions of Interest Analysis.** Two measures were computed to quantify the visual response in six clusters of body-part regions of interest (ROIs) outlined on group-average and single-subject maps. Each body-part ROI includes a set of vertices containing complex *F*-statistic values ($F_r$, $F_i$) enclosed in a 2D patch cut from an inflated cortical surface.

***Percentage of visual-tactile overlap.*** Visual-tactile overlap measures the percentage of vertices significantly activated by looming stimuli [$F(2, 230) = 4.7$, $P = 0.01$, uncorrected for single-subject maps; group mean $F(2, 230) = 3.04$, $P = 0.05$, uncorrected for group-average maps] in each body-part ROI. Fig. 3*D* shows the percentage of visual-tactile overlap in each ROI outlined on group-average maps in Fig. 3*B*. Fig. 3*E* shows the mean and SD of visual-tactile overlap percentages in ROIs across available subjects (Table S1 and Figs. S3 and S7) for each body-part cluster.

***Distribution of polar-angle representations.*** The distribution of polar-angle representations of the contralateral visual hemifield (−90° to 90°) among the vertices significantly activated by looming stimuli was computed in each body-part ROI. Fig. 3*F* shows box plots of the distribution of polar-angle representations in each body-part ROI outlined on group-average maps in Fig. 3*B*. Fig. 3*G* shows box plots of the distribution of polar-angle representations aggregated across available subjects (Table S1) for each group of body-part ROIs outlined on single-subject maps in Figs. S3 and S7.


1. Dale AM, Fischl B, Sereno MI (1999) Cortical surface-based analysis. I. Segmentation and surface reconstruction. *Neuroimage* 9(2):179–194.
2. Fischl B, Sereno MI, Dale AM (1999) Cortical surface-based analysis. II: Inflation, flattening, and a surface-based coordinate system. *Neuroimage* 9(2):195–207.
3. Collins DL, Neelin P, Peters TM, Evans AC (1994) Automatic 3D intersubject registration of MR volumetric data in standardized Talairach space. *J Comput Assist Tomogr* 18(2):192–205.
4. Hagler DJ, Jr, Riecke L, Sereno MI (2007) Parietal and superior frontal visuospatial maps activated by pointing and saccades. *Neuroimage* 35(4):1562–1577.


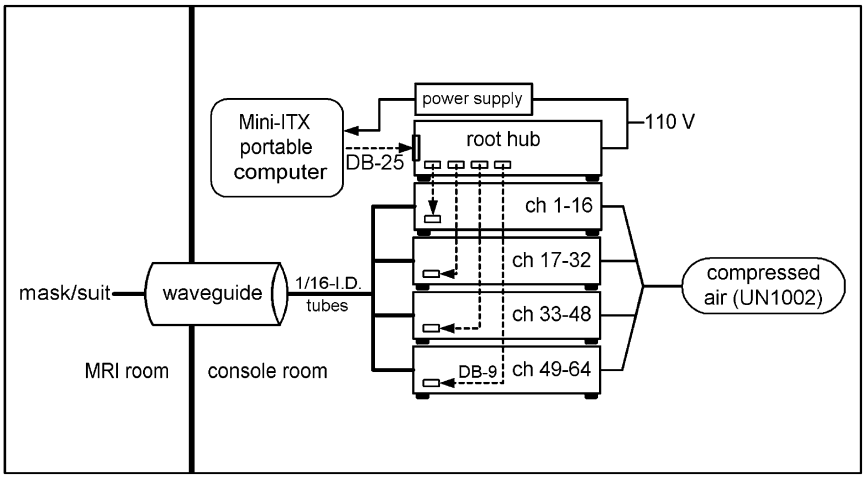


**Fig. S1.** Schematic diagram of the 64-channel pneumatic control system. The system consists of a portable computer, power supplies, a root hub, and four 16-channel pneumatic control modules. The root hub and pneumatic control modules (lower four boxes) are enclosed in stackable aluminum cases, which allow immediate expansion to 128 channels by adding another four modules. Stimulus generation programs written in C programming language sent 100-ms pulses of 8-bit transistor-transistor-logic (TTL) signals to the parallel port of a portable computer. A DB-25 cable connects the portable computer to the root hub. The root hub decoded incoming TTL signals to control (via DB-9 cables) the corresponding solenoid valves in the pneumatic control modules that received compressed air input (60–65 psi) from a gas cylinder (Praxair; UN1002). Thick branches exiting the pneumatic control modules indicate bundles of 64 tubes [1/16-inch inside diameter (I.D.)] that enter the MRI room via a waveguide and connect to the mask and suit on the subject.

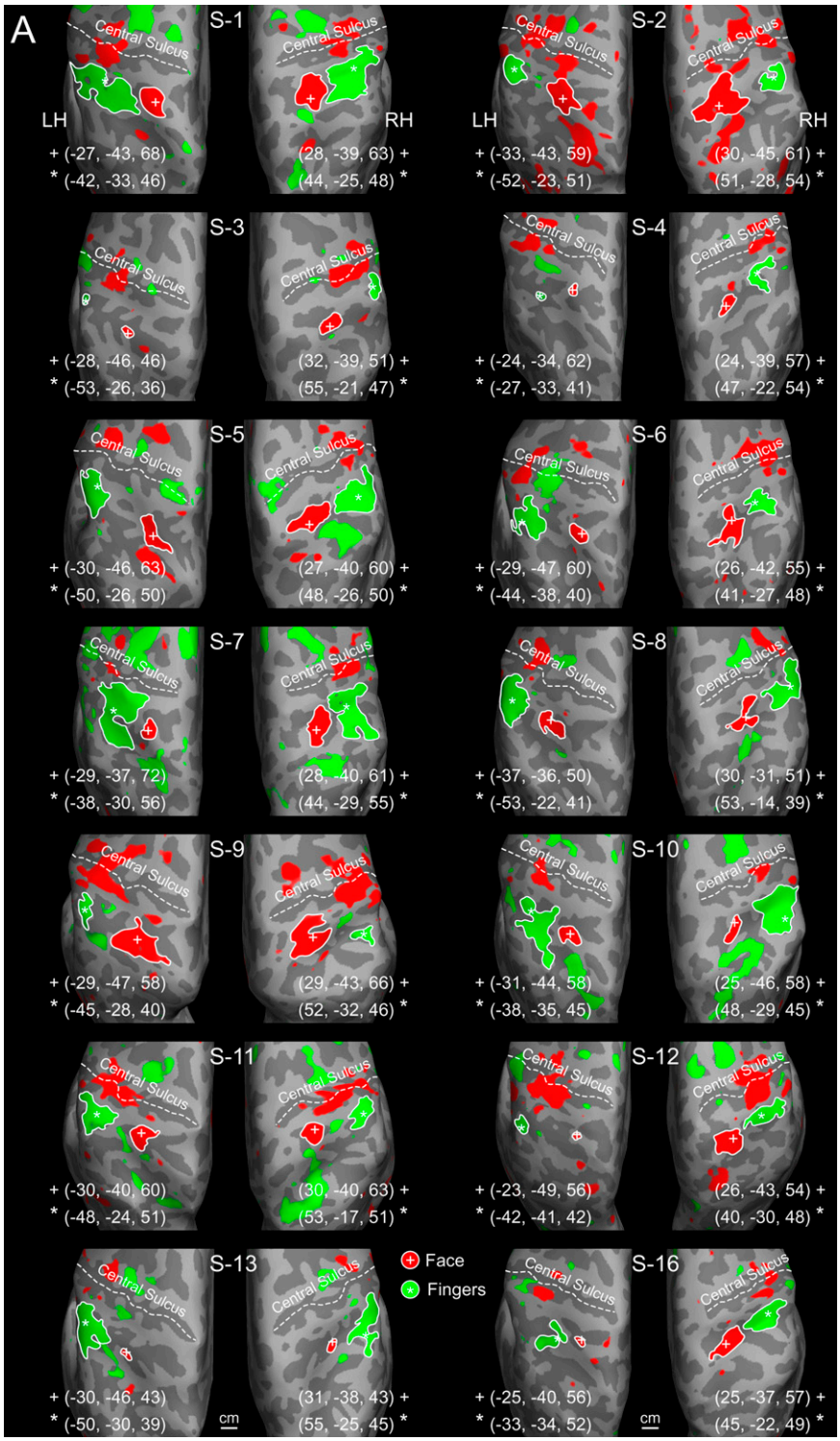


**Fig. S2.** (Continued)

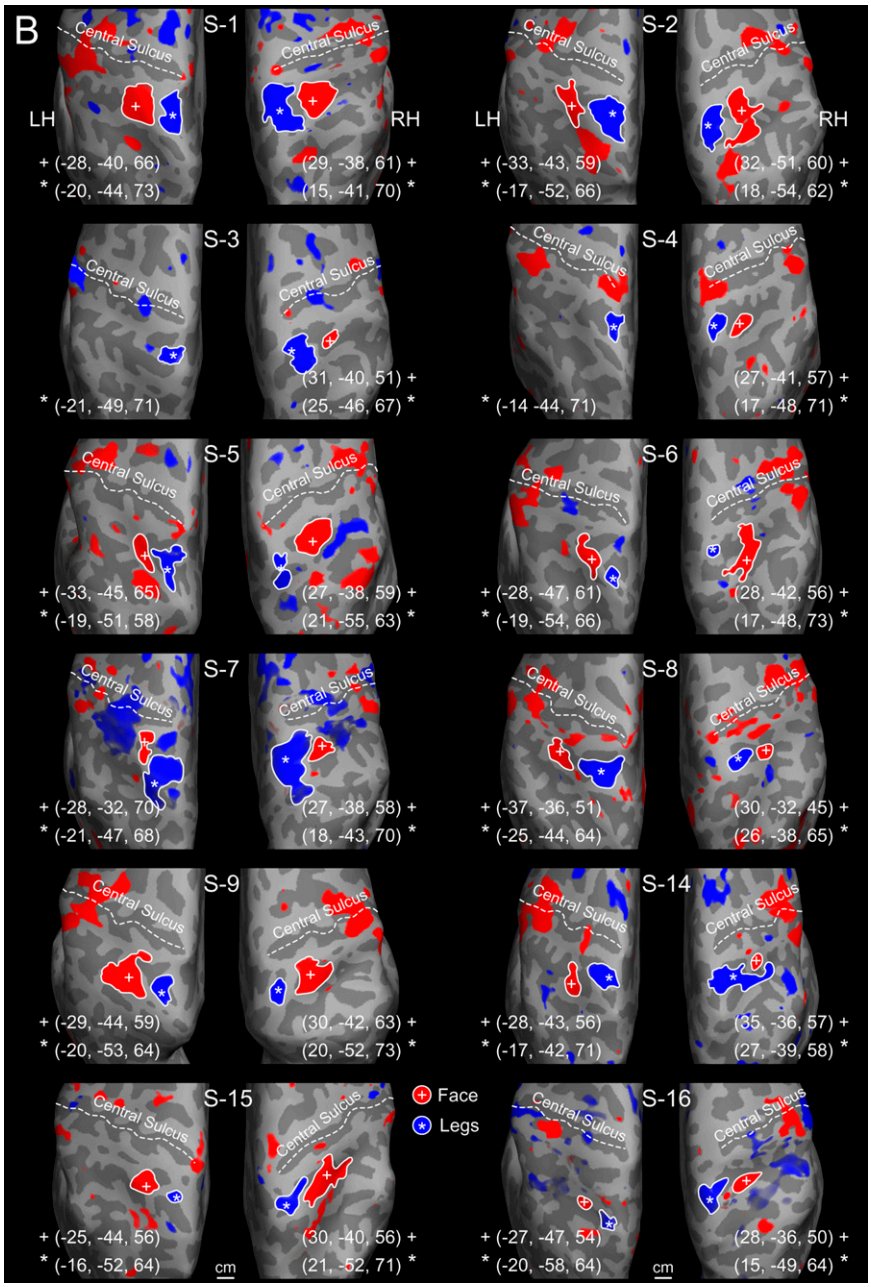


**Fig. S2.** (Continued)

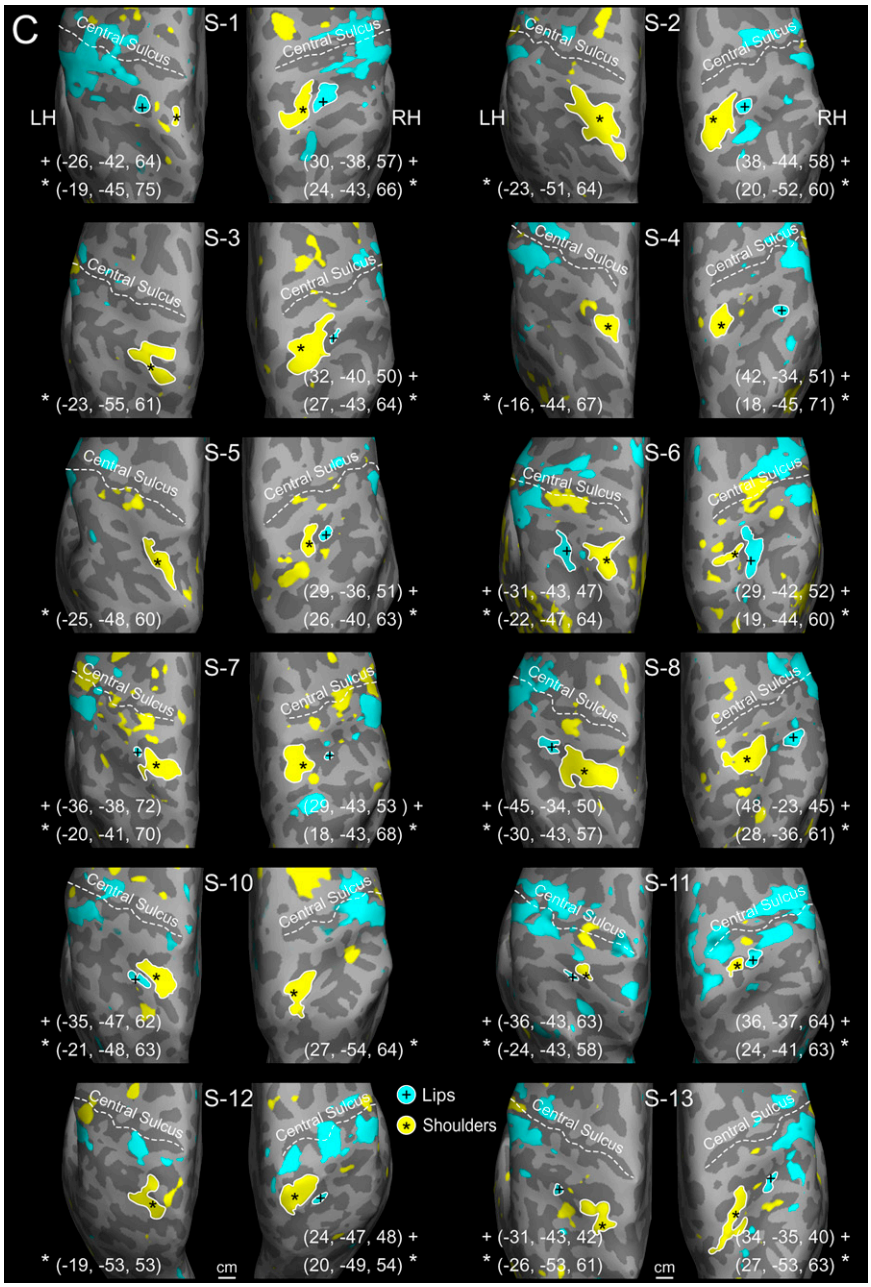


**Fig. S2.** (Continued)

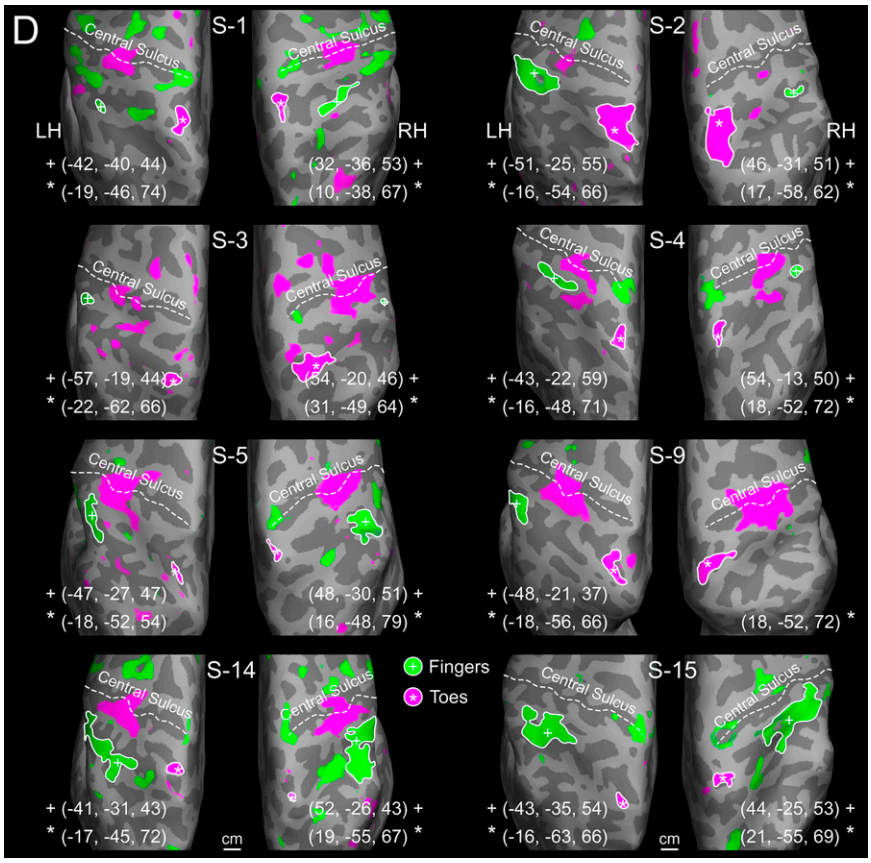


**Fig. S2.** Single-subject maps of body-part representations in superior posterior parietal cortex (PPC): (*A*) face vs. fingers scans ($n$ = 14); (*B*) face vs. legs scans ($n$ = 12); (*C*) lips vs. shoulders scans ($n$ = 12); (*D*) fingers vs. toes scans ($n$ = 8). Light and dark gray regions represent gyri and sulci on inflated cortical surfaces, respectively. White or black crosses (+) and asterisks (*) represent geometric centers of ROIs outlined in solid white contours. Talairach coordinates of ROI centers are listed as ($x$, $y$, z). S-#, subject index number; LH, left hemisphere; RH, right hemisphere.

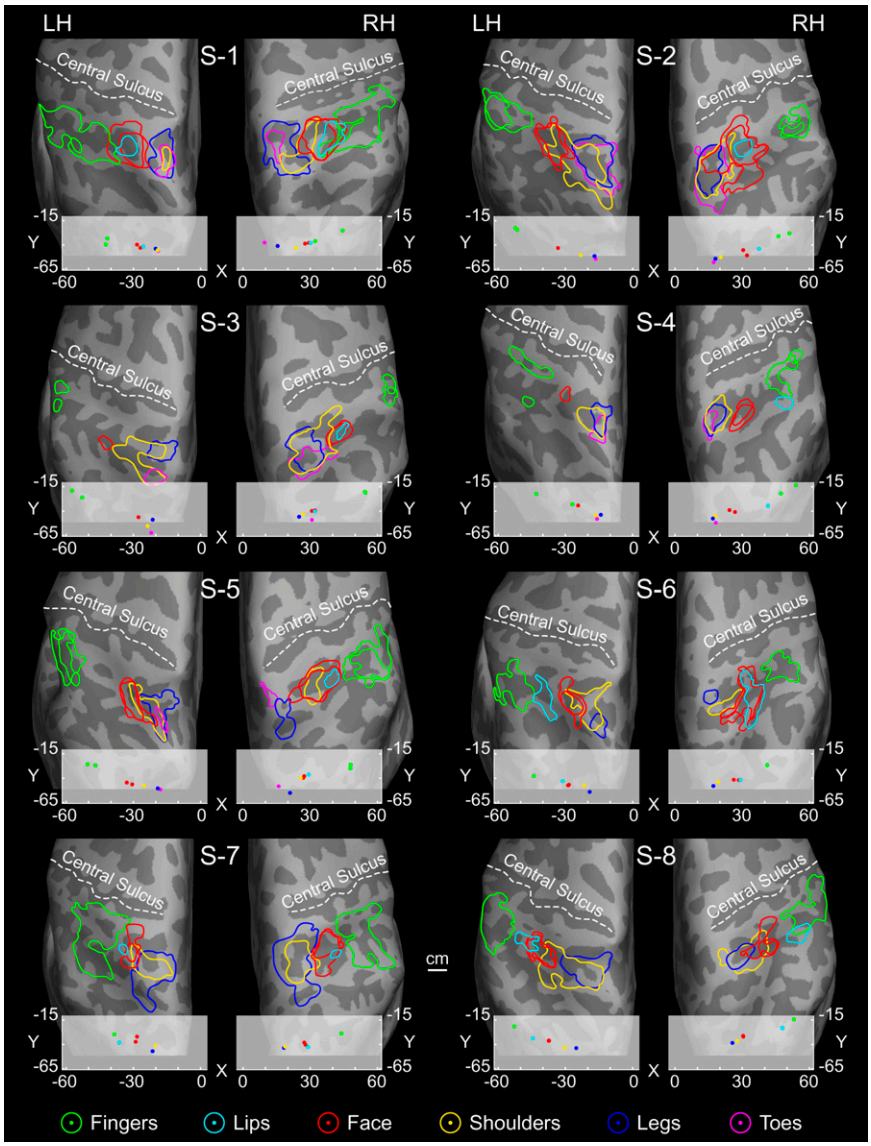


**Fig. S3.** (Continued)

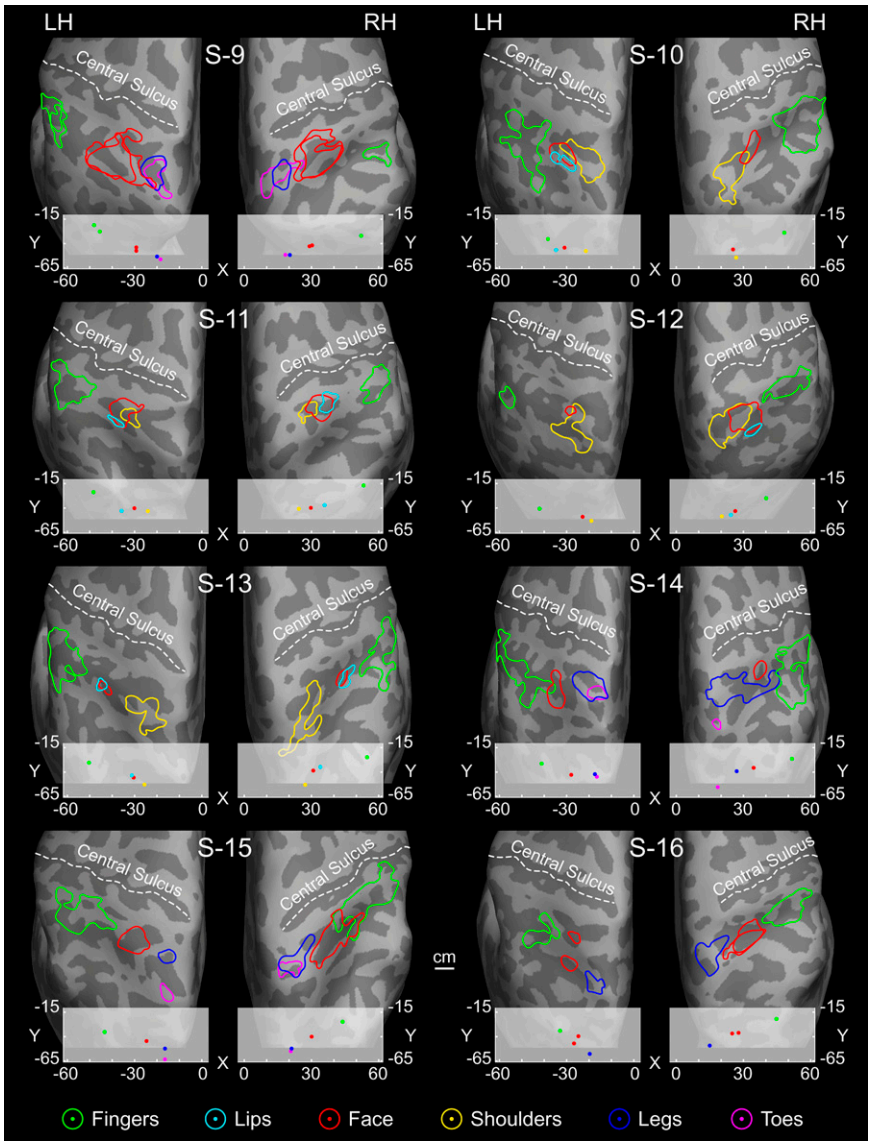


**Fig. S3.** Summary of single-subject body-part ROIs in superior PPC. Contours of body-part representations are redrawn from available subjects in Fig. S2. (*Insets*) ROI centers plotted on the *x*–*y* plane of Talairach coordinates. S-#, subject index number; LH, left hemisphere; RH, right hemisphere.

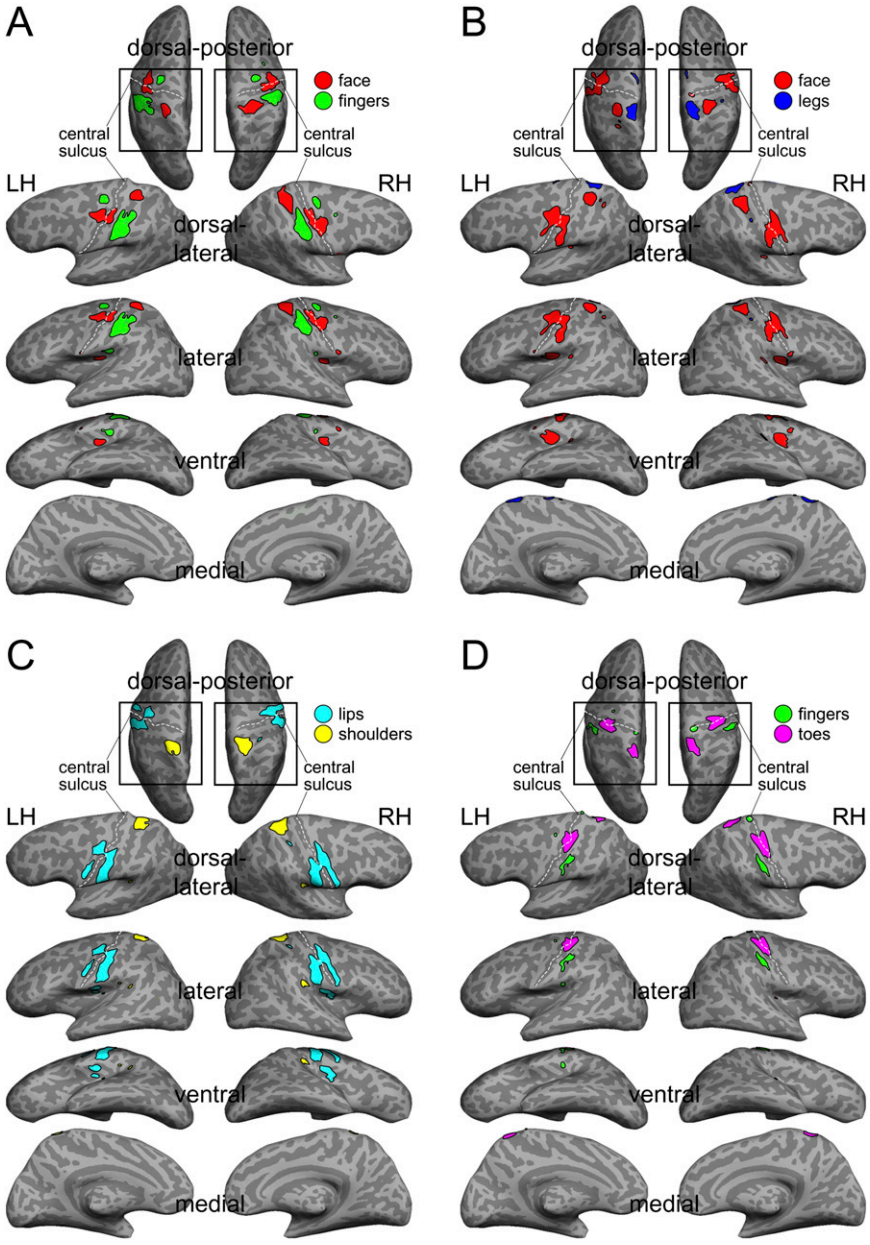


**Fig. S4.** Group-average maps of somatotopic activations displayed on subject 1's cortical surfaces: (*A*) face vs. fingers scans ($n$ = 14); (*B*) face vs. legs scans ($n$ = 12); (*C*) lips vs. shoulders scans ($n$ = 12); (*D*) fingers vs. toes scans ($n$ = 8).

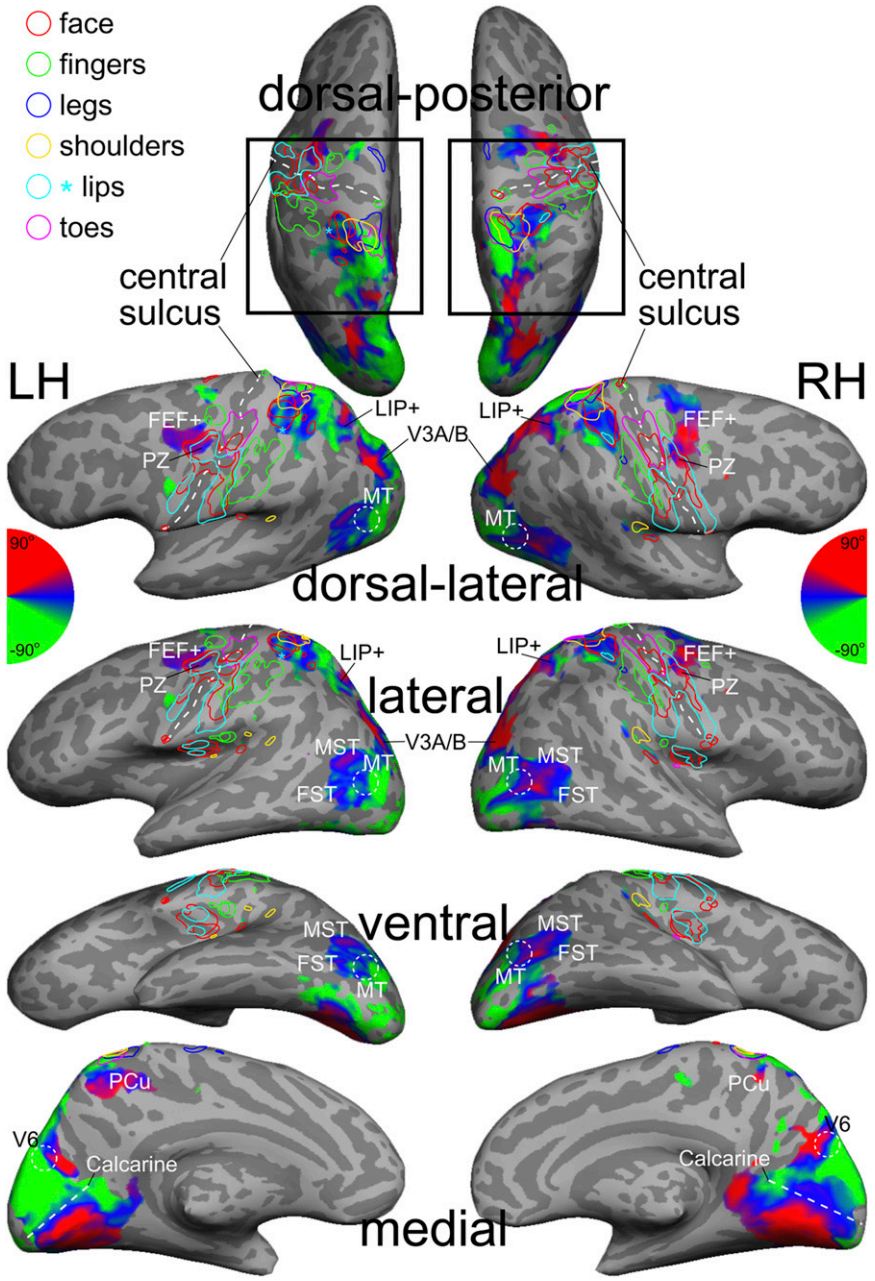


**Fig. S5.** Group-average somatotopic ROIs overlaid on group-average retinotopic maps displayed on subject 1's cortical surfaces. ROI contours are redrawn from Fig. S4. The cyan asterisk indicates the average ROI center of lip representations from available subjects ($n$ = 7) showing significant activations (Fig. S2*C* and Table S1). FEF+, frontal eye field complex; LIP+, lateral intraparietal complex; PZ, polysensory zone; MT/MST/FST, middle temporal motion areas; PCu, precuneus.

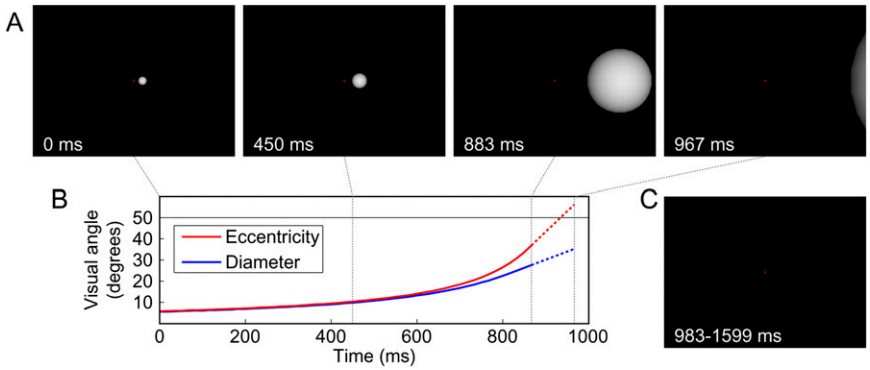


**Fig. S6.** Timing and dimension of a looming stimulus. The ball is looming along the right horizon in this representative trial. (*A*) Snapshots at key frames (60 frames/s) of the stimulus. Starting at 450 ms, the white ball randomly turns red in 20% of all trials. (*B*) Time courses of eccentricity and diameter of the ball. Eccentricity is defined as the visual angle between the central fixation and the center of the ball. Dashed traces represent the projected time courses after the ball enters the edge of the screen at 50° eccentricity, where a portion of the ball is still visible. (*C*) Fixation cross against a black background after the ball completely disappears at 983 ms.

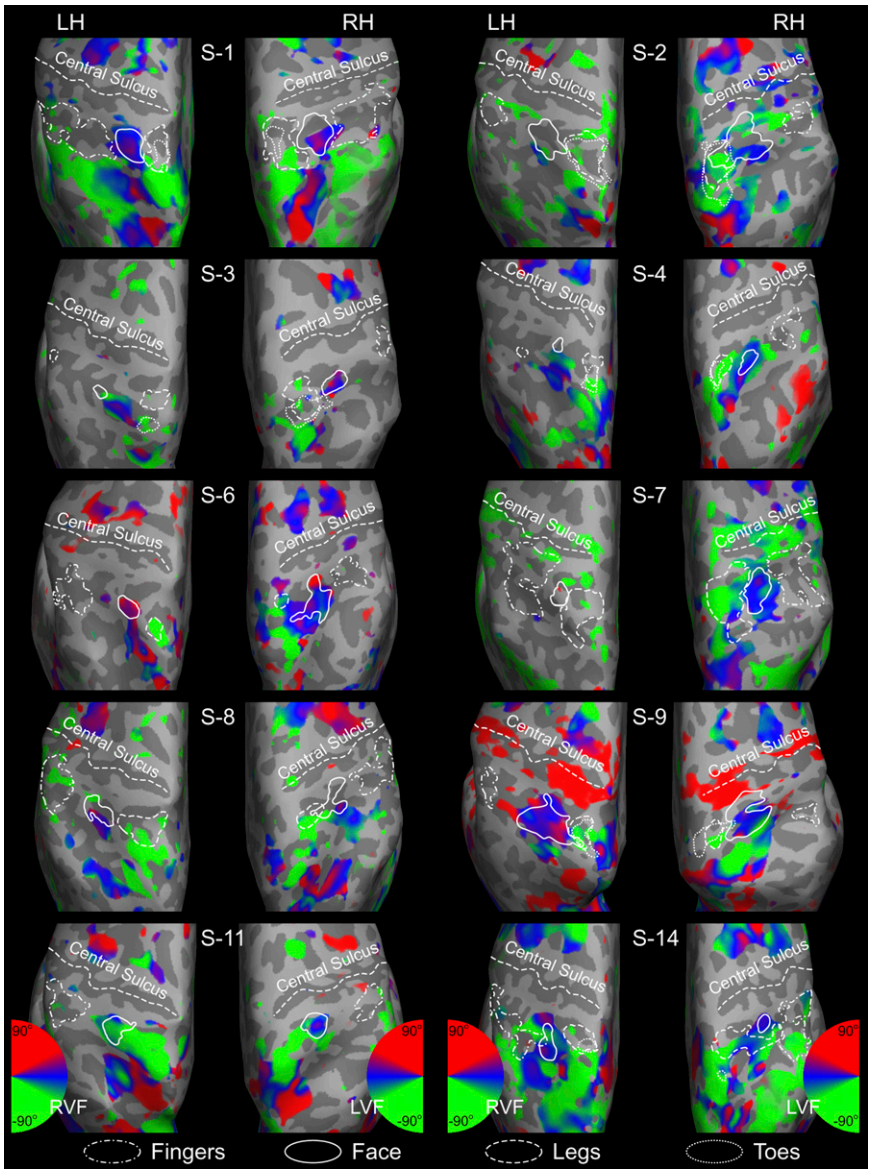


**Fig. S7.** Visual-tactile overlap in superior PPC. Retinotopic maps of 10 subjects are overlaid with the respective contours of four body-part ROIs (face, fingers, legs, and toes) from Fig. S3. Contours of shoulders and lips are not shown to reduce visual clutter. Color wheels, polar angle of the contralateral visual hemifield. S-#, subject index number. LH, left hemisphere; RH, right hemisphere. RVF, right visual field; LVF, left visual field.

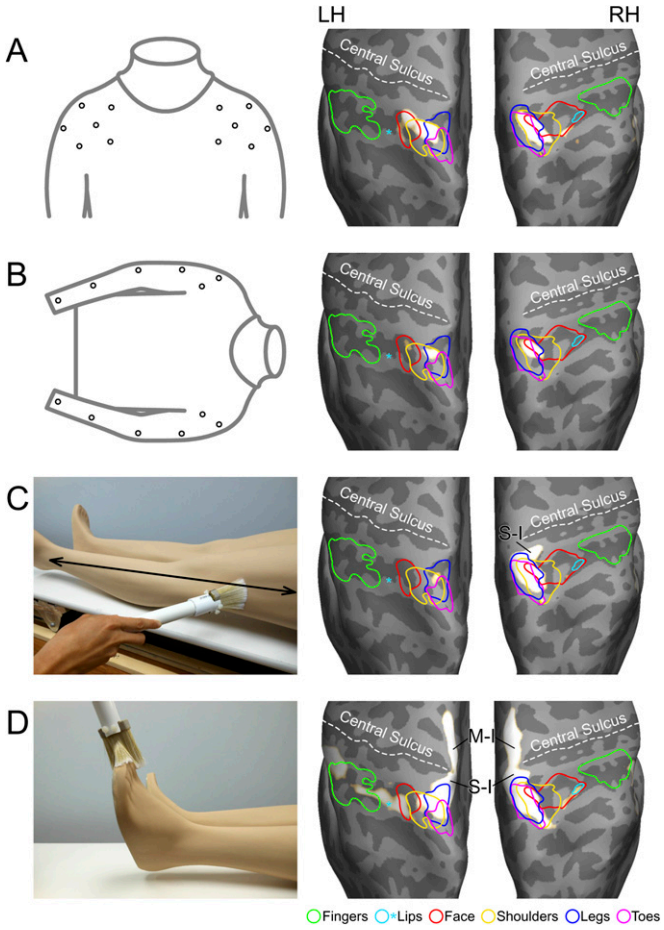


**Fig. S8.** Supplementary tactile experiments and results. (*A*) Shoulders. (*B*) Arms. (*C*) Left leg. (*D*) Toes. (*Left*) stimulation sites; (*Right*) group-average activation maps ($n$ = 8). Regions of significant activations [group mean $F(2, 102) = 3.09$, $P = 0.05$, uncorrected for (*A*–*C*); group mean $F(2, 102) = 10.09$, $P = 0.0001$, uncorrected for (*D*)] during stimulation periods are rendered in white on subject 1's cortical surfaces. Contours of group-average body-part ROIs over the activation maps were redrawn from Fig. 3*B*. LH, left hemisphere; RH, right hemisphere. S-I, primary somatosensory cortex; M-I, primary motor cortex.

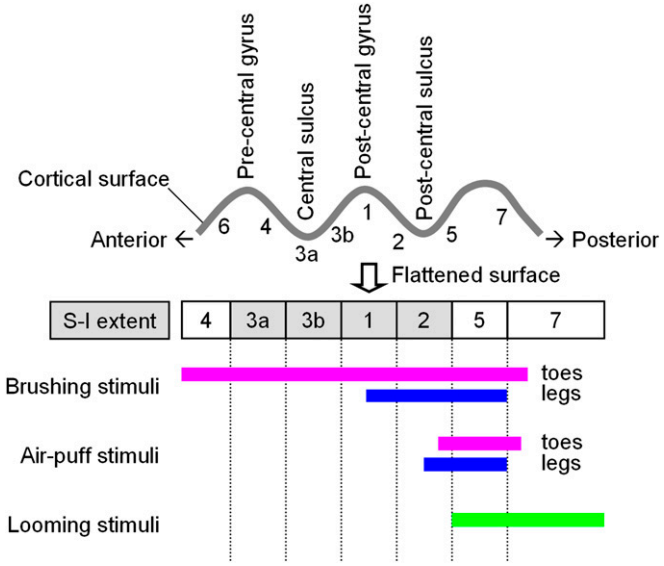


**Fig. S9.** Schematic illustration of activation extents across Brodmann's areas. Horizontal bars indicate activation extents driven by different modalities of stimuli as shown on group-average maps in Fig. 3*B* and Fig. S8. S-I, primary somatosensory cortex.

**Table S1. Distributions of Talairach coordinates of ROI centers for each body-part cluster**

| | Left hemisphere | | | Right hemisphere | | |
|---|---|---|---|---|---|---|
| Body parts | (*x*, *y*, *z*) | SD | *n* | (*x*, *y*, *z*) | SD | *n* |
| Face (+) | (−29, −44, 58) | 4.4 | 14 (10) | (29, −40, 58) | 3.3 | 14 (9) |
| Fingers (*) | (−44, −30, 46) | 3.6 | 14 (10) | (47, −25, 49) | 3.0 | 14 (10) |
| Face (+) | (−30, −43, 60) | 4.0 | 10 | (30, −40, 57) | 3.8 | 12 |
| Legs (*) | (−19, −49, 67) | 2.2 | 12 (9) | (20, −48, 67) | 2.7 | 12 (8) |
| Lips (+) | (−34, −41, 57) | 3.9 | 7 (5) | (34, −39, 52) | 5.3 | 11 (8) |
| Shoulders (*) | (−22, −47, 63) | 3.9 | 12 (8) | (23, −45, 63) | 2.4 | 12 (8) |
| Fingers (+) | (−46, −28, 48) | 4.2 | 8 | (46, −27, 50) | 5.4 | 6 |
| Toes (*) | (−17, −54, 67) | 3.9 | 8 (6) | (18, −51, 69) | 4.9 | 8 (6) |

(+) and (*) indicate the body parts stimulated during the first and second halves of each 32-s cycle in each two-condition paradigm, respectively. SD, SD of Euclidean distance from the center of each cluster; *n*, available subjects for each body-part cluster in Fig. S2 and group-average data in Fig. 3 *B*, *D*, and *F* and Figs. S4 and S5; number in parentheses, available subjects for each body-part cluster in Fig. 3 *E* and *G*.

**Table S2. Task performance in visual mapping sessions**

| Subject index | Average hit rate (%) | Average false response rate (%) | Average reaction time (ms) |
|---|---|---|---|
| 1 | 100 | 0.08 | 389 |
| 2 | 99.61 | 0 | 354 |
| 3 | 99.61 | 0.16 | 358 |
| 4 | 95.71 | 0.23 | 380 |
| 6 | 100 | 0.08 | 345 |
| 7 | 83.33 | 1.15 | 444 |
| 8 | 99.61 | 0.16 | 300 |
| 9 | 99.22 | 0.08 | 405 |
| 11 | 98.83 | 0.23 | 345 |
| 14 | 100 | 0 | 354 |
| Group mean | 97.59 | 0.22 | 367.4 |

Hit rate and reaction time were recorded from the 64 trials with red-ball targets in each scan and then averaged across four scans for each subject. Reaction time was measured from the moment the white ball turned red. Button presses recorded in the other 256 trials without targets were considered false responses.